


FSM-Net: An Efficient Frequency-Spatial Network for Real-World Deblurring

Vinh-Thuan Ly 

University of Science, VNU-HCM, Ho Chi Minh City, Vietnam
Vietnam National University, Ho Chi Minh City, Vietnam

22280092@student.hcmus.edu.vn

Abstract

Real-world image deblurring demands both high-fidelity restoration and computational efficiency, a balance existing methods often struggle to achieve. In this paper, we propose FSM-Net (Frequency-Spatial Multi-branch Network), a highly efficient solution that secured 2nd place in the NTIRE 2026 Challenge on Efficient Real-World Deblurring. FSM-Net pioneers a dual-domain approach: a novel Frequency Attention module explicitly recovers high-frequency structural details via FFT, while a Cross-Gated Vision E-Branchformer at the bottleneck captures global dependencies with linear complexity. To ensure robust convergence, we employ a progressive curriculum training strategy guided by a composite loss function (Multi-Scale Charbonnier, Structural Edge, and Frequency). Evaluated on the RSBlur benchmark, FSM-Net achieves an outstanding 33.144 dB PSNR with only 4.94M parameters and 159.35 GMACs (at 1920x1200 resolution). By effectively pushing the Pareto frontier of efficiency and quality, FSM-Net establishes a strong baseline for resource-constrained image restoration.

1. Introduction

Real-world image deblurring is a fundamental yet challenging task in computer vision, serving as a crucial pre-processing step for downstream applications like computational photography and autonomous driving [30, 33]. While early attempts heavily relied on perceptual losses [16] and Generative Adversarial Networks (GANs) [19], recent advancements have been dominated by Vision Transformers (ViTs) [11] and large-scale CNNs. Models such as SwinIR [23], IPT [3], and MAXIM [40] have pushed the boundaries of restoration quality. However, their massive parameter counts make them highly impractical for edge deployment.

The NTIRE 2026 Challenge on Efficient Real-World Deblurring [12] highlights a critical paradigm shift: modern networks must deliver high-fidelity restoration while strictly minimizing computational complexity. Existing architec-

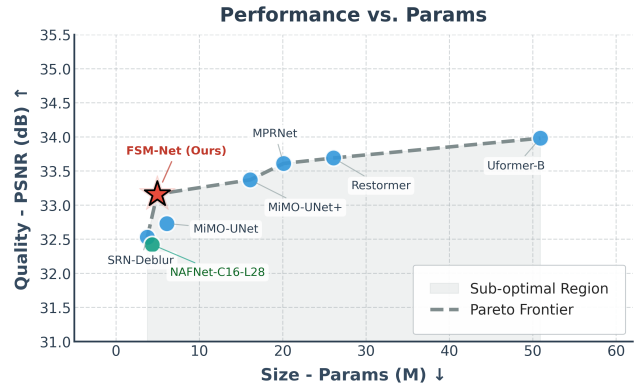


Figure 1. **Pareto Frontier on the RSBlur Benchmark.** FSM-Net pushes the limits of efficient real-world deblurring, establishing a new optimal trade-off between restoration quality and computational complexity. By explicitly decoupling frequency and spatial features, our 4.94 M parameter model delivers high-fidelity restoration (33.16 dB) that significantly outperforms standard baselines, while remaining vastly more efficient than heavy transformer architectures. FSM-Net secured 2nd place in the NTIRE 2026 Challenge.

tures often struggle with this dilemma, either sacrificing local structural details or relying on heavy self-attention mechanisms that scale quadratically with image resolution [5, 45]. As illustrated by the Pareto frontier in **Fig. 1**, balancing global context and local features without severe computational bottlenecks remains a major hurdle.

To tackle this challenge, we propose FSM-Net (Frequency-Spatial Multi-branch Network), an ultralightweight architecture built upon NAFNet [5]. Recognizing that severe motion blur fundamentally acts as a low-pass filter, we introduce a novel FSMBlock equipped with Frequency Attention. By applying Fast Fourier Transform (FFT), our model explicitly suppresses noise and enhances sharp edges directly in the frequency domain. Furthermore, we integrate a Cross-Gated Vision E-Branchformer Block at the network’s bottleneck. This module processes information through two parallel branches: a local CNN for precise

spatial detail recovery and a 4-head Transposed Attention branch for capturing global context with linear complexity.

Optimized via a robust composite loss, combining Multi-Scale Charbonnier Loss, Structural Edge Loss, and Frequency Consistency Loss, FSM-Net achieves an exceptionally lean profile. At a resolution of 1920×1200 , it requires only 4.94 M parameters and 159.35 GMacs, significantly pushing the Pareto frontier of efficient image restoration.

In summary, our main contributions are as follows:

- We introduce FSM-Net, an ultra-efficient architecture that seamlessly integrates spatial and frequency domain processing to optimize the trade-off between restoration quality and computational complexity.
- We design the novel FSMBlock with complex-valued Frequency Attention alongside a Cross-Gated Vision E-Branchformer Block, enabling the network to efficiently capture both global receptive fields and sharp local textures.
- We demonstrate the superiority of FSM-Net by achieving 33.144 dB PSNR on the NTIRE 2026 public test set, securing 2nd place and establishing a new efficiency benchmark for resource-constrained platforms.

2. Related Work

2.1. Deep Learning for Image Deblurring

Image deblurring has witnessed a paradigm shift with the rapid evolution of deep neural networks. Early approaches heavily relied on multi-stage or multi-scale Convolutional Neural Networks (CNNs) to progressively restore sharp details. Notable architectures such as SAPHNet [37], XYDeblur [14] MIMO-UNet [7], MPRNet [44], and HINet [4] achieved impressive spatial restoration by leveraging multi-input multi-output designs, cross-stage feature fusion, and instance normalization. Recently, transformers like Stripformer [39] Vision Transformers (ViTs)[11] have dominated low-level vision tasks. Restormer [45] introduced a highly effective Multi-Dconv Head Transposed Attention (MDTA) to reduce the quadratic complexity of standard self-attention, while Uformer [42] utilized window-based attention for local feature extraction. Despite their high Peak Signal-to-Noise Ratio (PSNR) on benchmark datasets, these attention-heavy models suffer from massive parameter counts and substantial latency. Recognizing this computational bottleneck, Chen et al. proposed NAFNet [5], which replaced non-linear activation functions with simple element-wise multiplications (SimpleGate), achieving competitive performance with significantly reduced FLOPs. Our FSM-Net builds upon the lightweight principles of NAFNet but dramatically enhances its representational capacity through targeted cross-domain feature extraction mechanisms.

2.2. Frequency-Domain and Hybrid Representations

Severe motion blur in real-world scenarios inevitably corrupts high-frequency structural details, which are notoriously difficult to recover using purely spatial convolutions. To address this, recent studies have begun exploring the frequency domain for image restoration. Methods utilizing the Fast Fourier Transform (FFT), such as Fast Fourier Convolution (FFC)[6] and Fourier Domain Adaptation (FDA)[43], have demonstrated that modulating amplitude and phase can effectively suppress noise and reconstruct sharp edges while enabling robust cross-domain generalization [15, 27].[18]. Furthermore, the integration of local CNNs and global attention mechanisms has proven to be a highly effective hybrid strategy. Architectures such as the Conformer [32] and E-Branchformer [17] in the speech and vision domains demonstrate that processing features through parallel local and global branches yields superior context modeling. Inspired by these advancements, our method introduces the Cross-Gated Vision E-Branchformer block alongside a complex-valued Frequency Attention module, allowing the network to explicitly decouple and learn high-frequency blur degradation patterns without incurring heavy computational overhead.

2.3. Efficient Restoration and NTIRE Challenges

The NTIRE workshops have consistently driven the boundaries of image restoration through rigorous challenges [12, 21, 22, 31, 47]. Historically, the pursuit of efficiency has leveraged lightweight convolutions [35] and structural re-parameterization[10]. Recent editions, including the 2025 Real-World Deblurring challenge[12], demonstrated remarkable inference speeds using highly optimized convolutional backbones. However, these spatial-only architectures often struggle with the long-range, non-uniform blur trajectories inherent in high-resolution imagery. To further push the Pareto frontier in the 2026 challenge, FSM-Net evolves this structural paradigm by integrating a hybrid frequency-spatial design. By decoupling spectral components via Frequency Attention and modeling global context with linear complexity, our model achieves superior restoration fidelity while maintaining the sub-second runtime requirements of mobile ISPs. This architectural advancement allows FSM-Net to handle complex degradations more robustly than prior lightweight spatial-only networks.

3. Methodology

To address the strict efficiency constraints of the NTIRE 2026 Challenge, we propose FSM-Net (Frequency-Spatial Multi-branch Network). Building upon the U-shaped NAFNet [5], we establish a Pareto balance between restoration quality and computational cost by completely redesign-

ing the feature extraction paradigm to explicitly decouple spatial textures and frequency components. This section details the overall pipeline, core architectural blocks, hybrid loss formulation, and training dynamics.

3.1. Overall Architecture

FSM-Net adopts a 4-level encoder-decoder architecture with dense skip connections. Given a blurry image $\mathbf{I}_{blur} \in \mathbb{R}^{3 \times H \times W}$, a 3×3 convolutional stem projects it into a shallow feature space $\mathbf{X}_0 \in \mathbb{R}^{C \times H \times W}$.

The encoder progressively downsamples features via strided convolutions (stride 2), doubling channels while halving spatial resolution to extract hierarchical representations. Both the encoder and decoder stages are exclusively populated with our proposed Frequency-Spatial Multi-branch Blocks (FSMBlock) to capture complex degradation patterns.

At the network bottleneck, where receptive fields are maximized but spatial dimensions are compressed, we introduce a sequence of Vision E-Branchformer Blocks to capture long-range semantic dependencies without inflating MACs. Finally, the decoder progressively upsamples deep features using PixelShuffle[36] to prevent checkerboard artifacts, culminating in a 3×3 convolution to predict the clean residual. The final sharp image is obtained via a global skip connection: $\mathbf{I}_{sharp} = \mathbf{I}_{blur} + \mathbf{R}_{pred}$.

3.2. Frequency-Spatial Multi-branch Block

Severe motion blur operates not only as a spatial distortion but fundamentally acts as a low-pass filter that severely degrades high-frequency structural details. Standard convolutions are inherently spatially biased and computationally inefficient for modeling such global frequency-domain degradations [8, 48]. Therefore, we design the FSMBlock, which augments the efficient SimpleGate mechanism [5, 9] with a novel Frequency Attention module.

Given an input feature map \mathbf{X}_{in} , we first apply Layer Normalization[1] followed by a 1×1 convolution for channel expansion. To capture long blur trajectories efficiently, we apply a depth-wise convolution with a large 7×7 kernel. Let the resulting intermediate feature be $\mathbf{X} \in \mathbb{R}^{C' \times H \times W}$. We split this feature along the channel dimension into two equal halves: \mathbf{X}_1 and \mathbf{X}_2 .

To explicitly recover high-frequency information, \mathbf{X}_2 is fed into the Frequency Attention module. We first transform \mathbf{X}_2 into the frequency domain using the 2D Real Fast Fourier Transform (rFFT):

$$\mathcal{F}(\mathbf{X}_2)(u, v) = \sum_{h=0}^{H-1} \sum_{w=0}^{W-1} \mathbf{X}_2(h, w) e^{-j2\pi(\frac{uh}{H} + \frac{vw}{W})} \quad (1)$$

where j is the imaginary unit. To modulate both the amplitude (contrast) and phase (structure) of the signal simulta-

neously, we define a learnable complex-valued weight parameter $\mathbf{W}_c \in \mathbb{C}^{1 \times C'/2 \times 1 \times 1}$. The frequency features are element-wise multiplied by this complex weight:

$$\mathbf{Z}_{fft} = \mathcal{F}(\mathbf{X}_2) \odot \mathbf{W}_c \quad (2)$$

The filtered complex signal is then transformed back to the spatial domain via the Inverse Fast Fourier Transform (irFFT), producing the enhanced feature $\tilde{\mathbf{X}}_2 = \mathcal{F}^{-1}(\mathbf{Z}_{fft})$. Unlike real-valued spectral filters that only scale the magnitude, our complex-valued weight \mathbf{W}_c enables simultaneous modulation of both amplitude and phase. Since motion blur fundamentally induces a phase shift and frequency-dependent attenuation, this dual-modulation capability allows FSM-Net to explicitly re-align shifted structural components while amplifying suppressed high-frequency signals. This spectral recalibration is crucial for resolving the ghosting artifacts typically found in non-uniform real-world blur. Finally, the output of the Frequency Attention is fused with the identity spatial branch (\mathbf{X}_1) using a non-linear gating mechanism:

$$\mathbf{X}_{gate} = \mathbf{X}_1 \odot \tilde{\mathbf{X}}_2 \quad (3)$$

Following this frequency-spatial gating, we introduce a Simplified Channel Attention (SCA) module to recalibrate the channel-wise feature responses and enhance the representational power. We first squeeze the spatial dimensions of \mathbf{X}_{gate} using Global Average Pooling (GAP) to obtain a channel descriptor $\mathbf{s} \in \mathbb{R}^{C'/2 \times 1 \times 1}$:

$$\mathbf{s}_c = \frac{1}{H \times W} \sum_{h=1}^H \sum_{w=1}^W \mathbf{X}_{gate}(c, h, w) \quad (4)$$

This global descriptor is then passed through a 1×1 convolution to capture cross-channel interactions without any dimensionality reduction. These weights are used to dynamically modulate the gated features: $\mathbf{X}_{sca} = \mathbf{X}_{gate} \odot \mathbf{W}_{sca}(\mathbf{s})$. Finally, \mathbf{X}_{sca} is projected back to the original channel dimension C via a 1×1 convolution (\mathbf{W}_{out}), and added to the residual identity mapping to form the intermediate feature:

$$\mathbf{X}_{mid} = \mathbf{X}_{in} + \mathbf{W}_{out}(\mathbf{X}_{sca}) \cdot \beta \quad (5)$$

where β is a learnable layer scaling parameter.

Subsequently, \mathbf{X}_{mid} is processed by a Feed-Forward Network (FFN) augmented with a SimpleGate to independently model channel-wise transformations. The final block output is obtained via a second residual connection:

$$\mathbf{X}_{out} = \mathbf{X}_{mid} + \text{FFN}(\mathbf{X}_{mid}) \cdot \gamma \quad (6)$$

where γ is another learnable scaling factor. By directly modulating the complex wave representations and recalibrating

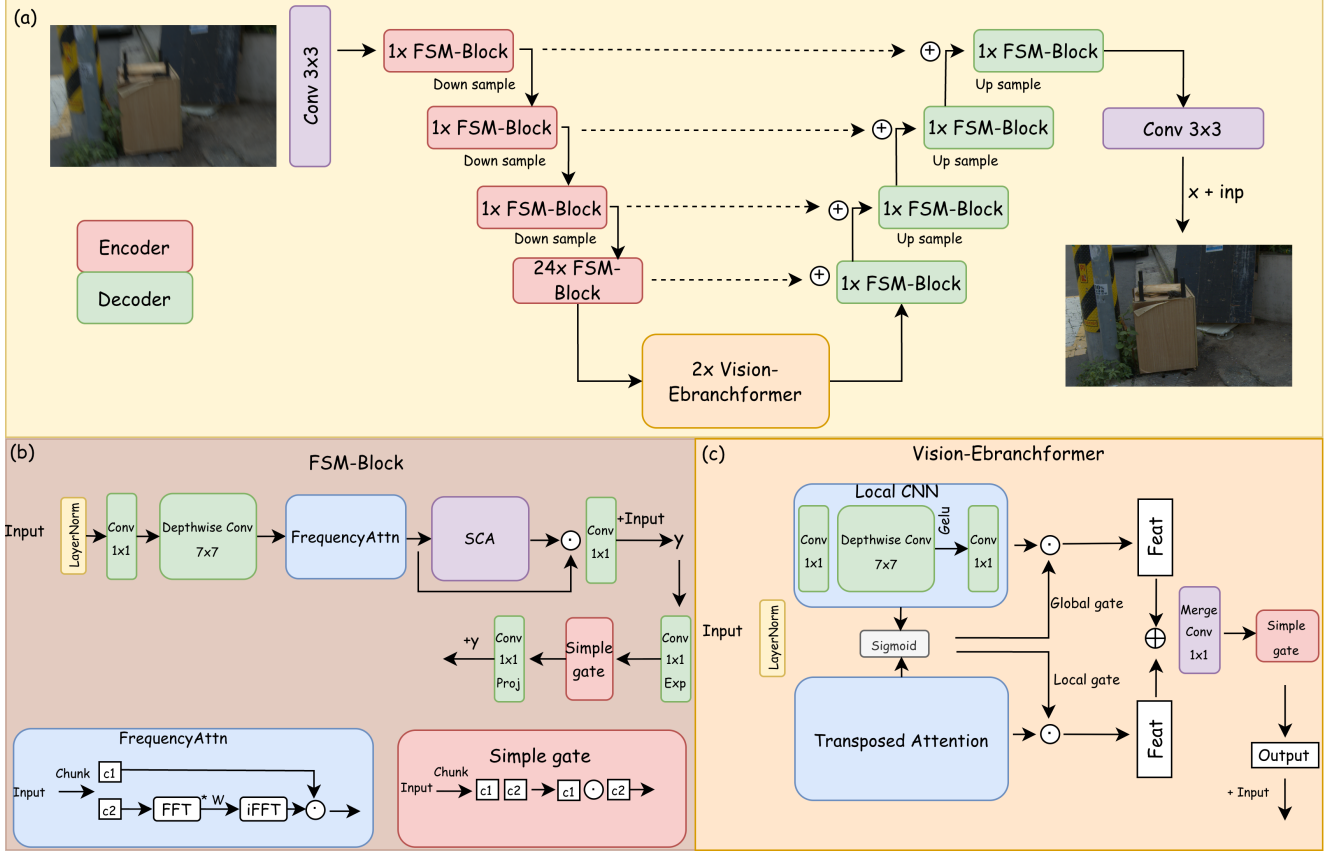


Figure 2. Overall Architecture of FSM-Net. Our model follows an efficient U-shaped hierarchical structure. (a) The global pipeline with 4-level encoder-decoder stages; (b) Detailed schematic of the Frequency-Spatial Multi-branch Block (FSMBlock) featuring Frequency Attention; (c) The Cross-Gated Vision E-Branchformer bottleneck designed for long-range dependency modeling with linear complexity.

brating channel dependencies, FSMBlock dynamically suppresses noise and sharpens edges with an $\mathcal{O}(N \log N)$ computational complexity, strictly adhering to the challenge’s efficiency requirements.

3.3. Cross-Gated Vision E-Branchformer Bottleneck

At the network’s bottleneck, capturing global context is paramount for resolving severe, large-scale blur. However, standard Self-Attention mechanisms scale quadratically with spatial resolution $\mathcal{O}(H^2W^2C)$, creating a severe computational bottleneck, while shifted-window variants [24] often lack sufficient receptive fields. To maintain the ultra-fast inference speed, we propose the Vision E-Branchformer Block, inspired by advancements in speech recognition [17], and adapt it for vision tasks through a novel cross-gating mechanism.

The block splits the normalized input into two parallel, complementary processing branches:

1. **Local CNN Branch:** Employs an inverted bottleneck structure to accurately model fine-grained spatial tex-

tures. It consists of a 1×1 expansion convolution, a 7×7 depth-wise convolution, a GELU activation[13], and a final 1×1 projection convolution, yielding local features \mathbf{F}_{loc} .

2. **Global Attention Branch:** Utilizes a 4-head Transposed Attention module. To inject local inductive bias into the attention mechanism, queries \mathbf{Q} , keys \mathbf{K} , and values $\mathbf{V} \in \mathbb{R}^{B \times \hat{C} \times HW}$ are first generated using a 3×3 depth-wise convolution. Instead of computing attention across the massive spatial dimension, we compute the covariance matrix across the channel dimension, inspired by Restormer[45]. Before the matrix multiplication, \mathbf{Q} and \mathbf{K} are \mathcal{L}_2 -normalized along the spatial dimension. The attention is computed as:

$$\mathbf{F}_{glob} = \text{Softmax} \left(\hat{\mathbf{Q}} \hat{\mathbf{K}}^T \cdot \tau \right) \mathbf{V} \quad (7)$$

where $\hat{\mathbf{Q}}$ and $\hat{\mathbf{K}}$ represent the normalized queries and keys, and τ is a learnable temperature parameter. This transposed formulation reduces the complexity from $\mathcal{O}(H^2W^2C)$ to $\mathcal{O}(HWC^2)$, making global context modeling extremely lightweight.

To synergize the representations from both domains, we introduce a Cross-Gating Mechanism. The features from one branch are utilized to generate attention gates for the other, facilitating mutual information exchange:

$$\mathbf{F}'_{loc} = \mathbf{F}_{loc} \odot \sigma(\mathbf{F}_{glob}) \quad (8)$$

$$\mathbf{F}'_{glob} = \mathbf{F}_{glob} \odot \sigma(\mathbf{F}_{loc}) \quad (9)$$

where $\sigma(\cdot)$ denotes the Sigmoid activation function. The mutually enhanced features are concatenated, projected via a 1×1 convolution, and refined through a SimpleGate module. Finally, the output is scaled by a learnable layer scaling parameter before being added to the residual stream.

3.4. Optimization Strategy

To optimize FSM-Net for complex real-world degradations, we employ a composite loss function that supervises the network across spatial, structural, and frequency domains. The total objective function \mathcal{L}_{total} is formulated as a weighted linear combination of three distinct loss components:

$$\mathcal{L}_{total} = w_1 \mathcal{L}_{MSC} + w_2 \mathcal{L}_{Edge} + w_3 \mathcal{L}_{FFT} \quad (10)$$

where w_1, w_2 , and w_3 are hyperparameters that balance the contribution of each domain during the training process.

Multi-Scale Charbonnier Loss (\mathcal{L}_{MSC}) To capture hierarchical dependencies and enforce spatial fidelity, we utilize a Multi-Scale Charbonnier Loss [2]. Computed across three scales $s \in \{1, 0.5, 0.25\}$ via average pooling on the predicted ($\hat{\mathbf{I}}$) and ground-truth (\mathbf{I}) images, the loss is defined as:

$$\mathcal{L}_{MSC} = \sum_s \frac{\gamma_s}{N_s} \sum_{i=1}^{N_s} \sqrt{(\hat{\mathbf{I}}_{s,i} - \mathbf{I}_{s,i})^2 + \epsilon^2} \quad (11)$$

where γ_s denotes the scale-specific weight parameter, N_s represents the total number of pixels at spatial scale s , i is the spatial pixel index, and $\epsilon = 10^{-12}$ is a small constant ensuring numerical stability. This hierarchical multi-scale supervision effectively encourages the network to restore both coarse global structures and fine-grained local textures.

Structural Edge Loss (\mathcal{L}_{Edge}) To explicitly enhance the sharpness of recovered boundaries, we introduce an Edge Loss based on the Laplacian operator Δ [28]. We minimize the Mean Squared Error (MSE) between the extracted high-frequency edges:

$$\mathcal{L}_{Edge} = \mathbb{E} \left[\left\| \Delta \hat{\mathbf{I}} - \Delta \mathbf{I} \right\|_2^2 \right] \quad (12)$$

By penalizing blurry edges, this component forces the model to prioritize sharp transitions and structural integrity in the restoration process.

Frequency Consistency Loss (\mathcal{L}_{FFT}) Motivated by the fact that motion blur is fundamentally a frequency-domain degradation[15], we penalize discrepancies in the Fourier space. We apply a Real Fast Fourier Transform (rFFT) to the spatial signals and minimize the \mathcal{L}_1 distance between their log-amplitudes:

$$\mathcal{L}_{FFT} = \mathbb{E} \left[\left\| \log(1 + |\mathcal{F}(\hat{\mathbf{I}})|) - \log(1 + |\mathcal{F}(\mathbf{I})|) \right\|_1 \right] \quad (13)$$

where $\mathcal{F}(\cdot)$ denotes the 2D rFFT operator. The logarithmic scaling ensures that the network remains sensitive to subtle differences in high-frequency spectral components, which are crucial for recovering sharp details in real-world blurry images.

3.5. Exponential Moving Average

To ensure training stability and improve generalization without incurring test-time overhead, we integrate Exponential Moving Average (EMA)[29]. EMA acts as a temporal ensemble, smoothing noisy gradient updates. Let $\theta^{(t)}$ be the model weights at training step t , the EMA weights $\theta_{EMA}^{(t)}$ are updated as:

$$\theta_{EMA}^{(t)} = \alpha \theta_{EMA}^{(t-1)} + (1 - \alpha) \theta^{(t)} \quad (14)$$

where the decay rate α is empirically set to 0.999. This mechanism acts as a low-pass filter in the parameter space, dampening weight oscillations and guiding optimization toward wider, *flat minima*. Consequently, EMA significantly enhances the model’s robustness against domain shifts, ensuring stable and high-fidelity restoration on unseen test distributions.

4. Experiments

In this section, we provide a comprehensive evaluation of the proposed FSM-Net. We describe the dataset used for the challenge, the intricate multi-stage training details, and present our results in comparison with state-of-the-art methods.

4.1. Dataset and Evaluation Metrics

RSBlur Dataset: We conduct our experiments on the RS-Blur dataset [34], the official dataset for the NTIRE 2026 Efficient Real-World Deblurring Challenge. To bridge the domain gap between synthetic and real-world degradations, RSBlur employs a sophisticated blur synthesis pipeline. Instead of relying on naive artificial blur kernels, it utilizes real-world sharp image sequences and accurately models the physical camera image formation process, incorporating factors such as sensor noise, saturation, and signal processing pipelines, to synthesize highly realistic blurry/sharp training pairs. The dataset contains diverse indoor and outdoor scenes with complex motion blur patterns. For our



Figure 3. **Visual results of FSM-Net on the NTIRE 2026 test set.** We present several representative examples to demonstrate the restoration capability of our proposed architecture. FSM-Net effectively recovers sharp structural details and suppresses complex motion artifacts, contributing to our 2nd place ranking on the official public leaderboard. These results highlight the model’s efficacy in resolving diverse real-world blurring trajectories. Zoom in for better visualization.

training, we utilize the provided training split, consisting of high-resolution image pairs, and evaluate our performance on the full test set.

Evaluation Metrics: To quantitatively assess the restoration quality, we utilize the Peak Signal-to-Noise Ratio (PSNR), Structural Similarity Index (SSIM) [41] and Learned Perceptual Image Patch Similarity (LPIPS)[46]. Furthermore, following the challenge mandates, we measure the Runtime per image on a standard GPU to ensure the efficiency of our model. All metrics are calculated in the RGB color space.

4.2. Implementation Details

Network Configuration: The proposed FSM-Net is configured with a base channel width $C = 16$. The encoder-decoder depths are set to $[1, 1, 1, 24]$ and $[1, 1, 1, 1]$, respectively, with the number of middle blocks Vision E-Branchformer set to 2 at the bottleneck. This asymmetric design prioritizes deep feature extraction at lower resolutions to maintain a small computational footprint.

Optimizer and Scheduler: We employ the AdamW optimizer[26] with $\beta_1 = 0.9, \beta_2 = 0.999$ and a weight decay of 10^{-4} . The initial learning rate is set to 10^{-4} and is decayed to 10^{-6} using a Cosine Annealing scheduler[25]. To ensure numerical stability and memory efficiency, we utilize Automatic Mixed Precision (AMP) with `float16` during the entire training process. Furthermore, an Exponential Moving Average (EMA) with a decay rate of 0.999 is applied to the model weights to stabilize convergence and enhance generalization.

Multi-stage Curriculum Training: We implement a 5-phase progressive training strategy over 400 epochs to facilitate convergence from coarse structures to fine textures:

- **Phase 1 (Epochs 0-20):** We utilize a crop size of 512×512 and optimize solely with the Multi-Scale Charbonnier Loss ($w_1 = 1.0, w_2 = 0, w_3 = 0$) to establish a stable initial spatial mapping.
- **Phase 2 (Epochs 20-120):** Maintaining the 512×512 resolution, we activate the structural and frequency losses ($w_2 = 0.01, w_3 = 0.005$) to begin capturing high-frequency details.
- **Phase 3 (Epochs 120-220):** The crop size is increased to 1024×1024 to allow the model to learn long-range motion blur trajectories while keeping the loss configuration constant.
- **Phase 4 (Epochs 220-290):** We transition to a 1280×720 resolution and increase the loss weights to $w_2 = 0.05$ and $w_3 = 0.01$ for more aggressive edge and frequency refinement.
- **Phase 5 (Epochs 290-400):** In the final stage, we train on the near-original resolution of 1920×1200 until convergence, ensuring the model is fully adapted to the high-resolution inference requirements of the challenge.

The entire training is conducted on a system equipped with a single NVIDIA RTX 5090 GPU. We utilize a batch size of 4 for Phases 1 through 4. In Phase 5, to accommodate the near-original resolution (1920×1200) within the VRAM constraints while maintaining high-fidelity feature maps, the batch size is adjusted to 2.

4.3. Main Results

We evaluated FSM-Net on the NTIRE 2026 Efficient Real-World Deblurring Public Test Set, which features complex degradations to test restoration limits under strict compu-

Table 1. **NTIRE 2026 Efficient Real-World Deblurring Challenge Results (Public test Phase)**. Methods are ranked by PSNR. The top three identical submissions are grouped as a single entity. Our FSM-Net secures a highly competitive 2nd place overall, offering a highly optimized and fully reported sub-second runtime. The runtime of 0.276s for FSM-Net corresponds to the $TTA \times 4$ ensemble strategy, which was used for the final submission.

Rank	Team Name	PSNR \uparrow	SSIM \uparrow	Time (s) \downarrow
1	jingjing et al.	33.390	0.8585	N/A*
2	RobinLy (Ours)	33.144	0.8516	0.276
3	weichow	32.883	0.8467	N/A*
4	licheng	32.805	0.8473	N/A*
5	zzhlttcy	32.657	0.8450	N/A*
6	zhouzhaorun	32.593	0.8422	N/A*
7	berryzis	32.322	0.8394	N/A*
8	geometric_ai	32.216	0.8371	0.78

tational constraints. As summarized in Table 1, FSM-Net secured 2nd place overall with a PSNR of 33.144 dB and an SSIM of 0.8516. This validates our core hypothesis: integrating the Frequency Attention module and Cross-Gated Vision E-Branchformer significantly enhances representational capacity without computationally prohibitive network scaling.

Crucially, FSM-Net establishes a highly practical Pareto balance between restoration quality and computational cost. Achieving its peak performance with an optimized latency of just 0.276s, our model operates significantly faster than other top-ranking submissions reporting runtimes (e.g., Rank 8 at 0.78s). This sub-second efficiency highlights its strong potential for real-time edge deployment.

Furthermore, FSM-Net outperforms the defending 2025 challenge champion (*licheng*, ranked 4th this year with a PSNR of 32.805 dB) by a substantial margin of +0.339 dB. This leap underscores the superiority of our dual-domain processing paradigm, demonstrating that our frequency-spatial decoupling effectively breaks the performance ceilings of prior spatial-only architectures.

Comprehensive SOTA Benchmark and Cross-Dataset Generalization To rigorously evaluate FSM-Net, we present a comprehensive benchmark against state-of-the-art (SOTA) deblurring methods. This evaluation is twofold: assessing restoration efficacy on the official RSBlur public full test set (3,360 real-world image pairs) and analyzing cross-domain generalization on three diverse external datasets (RealBlur-R, RealBlur-J, and GoPro).

As detailed in Table 2, FSM-Net achieves high-fidelity restoration on the RSBlur benchmark with a PSNR of 33.16 dB and an SSIM of 0.8533. It is crucial to emphasize that these metrics are obtained using a direct, single forward pass without the aid of any Test-Time Augmentation (TTA). Notably, FSM-Net delivers this competitive, unaugmented performance while requiring a mere fraction of the com-

putational footprint (4.94M parameters) compared to heavy SOTA architectures like MPRNet[44] or Uformer-B[42].

Furthermore, to validate cross-domain adaptability, we initialized FSM-Net with our best RSBlur pre-trained weights and performed a lightweight fine-tuning of merely 5 epochs on the external benchmarks. Despite this minimal adaptation phase, FSM-Net exhibits rapid convergence and robust generalizability. On the real-world RealBlur-R and RealBlur-J[33] datasets, our method achieves 36.95 dB and 29.45 dB respectively, remaining highly competitive with baselines specifically trained on those domains. Simultaneously, its stable performance on the synthetic GoPro dataset underscores that the representational capacity established by our frequency-spatial decoupling paradigm transfers effectively to unseen motion blur trajectories without severe overfitting.

Visual Performance Analysis Figure 3 presents a qualitative evaluation on the NTIRE 2026 test set, demonstrating FSM-Net’s capability to mitigate severe motion artifacts. Specifically, our Frequency Attention module accurately reconstructs dense high-frequency details, such as legible text on the “Mr.Pizza” signage and sharp license plates, by explicitly eliminating ghosting artifacts. For large-scale geometries subjected to long blur trajectories (e.g., playground equipment and the waterfront monument), the Cross-Gated Vision E-Branchformer successfully restores structural integrity without warping. Furthermore, our Multi-Scale Charbonnier Loss ensures background regions like the sky and foliage remain perceptually smooth, preventing the over-sharpening halos common in traditional methods. These qualitative improvements directly corroborate our quantitative success (2nd place, PSNR: 33.144 dB, SSIM: 0.8516).

4.4. Ablation Study

Architectural Components Ablation: To rigorously evaluate the individual contributions of our proposed modules under strict computational constraints, we conducted an accelerated 20-epoch ablation study at high resolution (1920×1200) using the 3,360 sample full test set. As shown in Table 3, the spatial-only baseline (NAFNet)[5] establishes a foundation at 31.39 dB PSNR. Integrating the Frequency Attention (FAtn) module yields a noticeable improvement to 31.57 dB, demonstrating the necessity of explicit spectral recalibration for mitigating high-frequency motion artifacts. Alternatively, deploying the Vision E-Branchformer (Ebranch) enhances spatial long-range dependency modeling, elevating the performance to 31.60 dB.

Crucially, when both pathways are synergized in the full FSM-Net, the restoration quality peaks at 31.83 dB with a highly competitive LPIPS of 0.3456. Notably, this combined improvement (+0.44 dB over the baseline) strictly

Table 2. **Comprehensive Benchmark of State-of-the-Art Methods Across Multiple Datasets.** For cross-dataset evaluation (RealBlur-R, RealBlur-J, and GoPro), FSM-Net was fine-tuned for only 5 epochs from the RSBlur pre-trained weights. “-” indicates that the metric or result is not explicitly reported or available for that specific configuration. FSM-Net achieves an exceptional balance between high-fidelity restoration and computational efficiency across diverse real-world and synthetic degradation profiles.

Method	Param (M)↓	Dataset Performance (PSNR ↑ / SSIM ↑)			
		RSBlur	RealBlur-R	RealBlur-J	GoPro
SRN-Deblur [38]	3.76	32.53 / 0.8398	38.65 / 0.9652	31.38 / 0.9091	28.36 / 0.9150
NAFNet-C16-L28[5]	4.35	32.42 / 0.8400	-	-	-
DeblurGAN-v2 [20]	6.09	-	36.44 / 0.9347	29.69 / 0.8703	-
MiMO-UNet [7]	6.10	32.73 / 0.8457	-	-	-
MiMO-UNet+ [7]	16.1	33.37 / 0.8560	-	-	-
MPRNet [44]	20.1	33.61 / 0.8614	-	-	30.96 / 0.9390
Nah <i>et al.</i> [30]	22.6	-	32.51 / 0.8406	27.87 / 0.8274	29.08 / 0.9135
Restormer [45]	26.1	33.69 / 0.8628	-	-	31.22 / 0.9420
Uformer-B [42]	50.9	33.98 / 0.8660	-	-	30.83 / 0.9520
FSM-Net (Ours)	4.94	33.16 / 0.8533	36.95 / 0.9585	29.45 / 0.8840	30.60 / 0.9068

Table 3. **Architectural Ablation.** Evaluated on 3,360 images after a 20 epoch high resolution training schedule.

Model	FAttn	Ebranch	Param (M)	MACs (G)	PSNR↑	SSIM↑	LPIPS↓
Baseline	×	×	4.35	146.33	31.39	0.8175	0.3557
+ FAttn	✓	×	4.66	155.66	31.57	0.8217	0.3494
+ Ebranch	×	✓	4.93	159.35	31.60	0.8216	0.3478
FSM-Net	✓	✓	4.94	159.35	31.83	0.8282	0.3456

Table 4. **Ablation Study on Test-Time Augmentation (TTA) Strategies.** The trade-off between restoration quality (PSNR/SSIM) and computational efficiency (Latency) evaluated on the RSBlur full test set. Latency is measured on a single NVIDIA RTX 5090 GPU.

TTA	Transforms	PSNR↑	SSIM↑	Time (s)↓
×1	None	33.006	0.8500	0.069
×2	+ H-Flip	33.105	0.8510	0.138
×3	+ V-Flip	33.135	0.8515	0.207
×4	+ D-Flip	33.144	0.8516	0.276

exceeds the sum of their individual marginal gains (+0.18 dB and +0.21 dB). This non-linear performance boost empirically proves that our frequency and spatial modules are highly complementary, successfully capturing orthogonal degradation features rather than redundant information. From an efficiency standpoint, this substantial perceptual and quantitative leap incurs only a marginal computational overhead (+0.59 M parameters, +13.02 GMacs). This firmly validates that our dual-domain design fundamentally expands the network’s representational capacity without violating the strict boundaries of efficient deployment.

Test-Time Augmentation (TTA) Trade-offs: To maximize restoration quality within the sub-second constraint, we evaluate four progressive TTA configurations (Table 4). The baseline (TTA ×1) achieves an ultra-fast 0.069s latency with a competitive 33.006 dB PSNR. Progressively incorporating horizontal (TTA ×2) and vertical (TTA ×3) flips yields consistent PSNR gains. For the full ensemble (TTA ×4, including a diagonal flip), we implement a weighted blending strategy (0.4 for the original, 0.2 for each augmentation) rather than a naive mean. This preserves the original spatial cues, achieving a peak PSNR of 33.144 dB at 0.276s. Ultimately, this demonstrates that FSM-Net can dynamically adapt to strict latency budgets (0.07s–0.28s) without any architectural modifications.

5. Conclusion

In this paper, we presented FSM-Net, an ultra-efficient frequency-spatial multi-branch architecture tailored for real-world image deblurring. By synergizing spatial-domain convolutions with complex-valued Frequency Attention, our model establishes a new Pareto frontier, achieving a superior balance between high-fidelity restoration and low computational overhead. With only 4.94 M parameters and a lean complexity of 159.35 GMacs at 1920 × 1200 resolution, FSM-Net addresses the critical requirements for high-resolution processing in resource-constrained environments. The proposed method demonstrated outstanding performance during the NTIRE 2026 challenge, currently securing 2nd place on the public leaderboard with a PSNR of 33.144 dB. FSM-Net thus establishes a strong, efficient baseline for future research in resource-constrained high-fidelity image restoration.

References

- [1] Jimmy Lei Ba, Jamie Ryan Kiros, and Geoffrey E. Hinton. Layer normalization, 2016. 3
- [2] P. Charbonnier, L. Blanc-Feraud, G. Aubert, and M. Barlaud. Two deterministic half-quadratic regularization algorithms for computed imaging. In *Proceedings of 1st International Conference on Image Processing*, pages 168–172 vol.2, 1994. 5
- [3] Hanting Chen, Yunhe Wang, Tianyu Guo, Chang Xu, Yiping Deng, Zhenhua Liu, Siwei Ma, Chunjing Xu, Chao Xu, and Wen Gao. Pre-trained image processing transformer. In *Proceedings of the IEEE/CVF Conference on Computer Vision and Pattern Recognition (CVPR)*, pages 12299–12310, 2021. 1
- [4] Liangyu Chen, Xin Lu, Jie Zhang, Xiaojie Chu, and Chengpeng Chen. Hinet: Half instance normalization network for image restoration. In *Proceedings of the IEEE/CVF Conference on Computer Vision and Pattern Recognition (CVPR) Workshops*, pages 182–192, 2021. 2
- [5] Liangyu Chen, Xiaojie Chu, Xiangyu Zhang, and Jian Sun. Simple baselines for image restoration. In *Computer Vision – ECCV 2022: 17th European Conference, Tel Aviv, Israel, October 23–27, 2022, Proceedings, Part VII*, page 17–33, Berlin, Heidelberg, 2022. Springer-Verlag. 1, 2, 3, 7, 8
- [6] Lu Chi, Borui Jiang, and Yadong Mu. Fast fourier convolution. In *Advances in Neural Information Processing Systems*, pages 4479–4488. Curran Associates, Inc., 2020. 2
- [7] Sung-Jin Cho, Seo-Won Ji, Jun-Pyo Hong, Seung-Won Jung, and Sung-Jea Ko. Rethinking coarse-to-fine approach in single image deblurring. In *Proceedings of the IEEE/CVF International Conference on Computer Vision (ICCV)*, pages 4641–4650, 2021. 2, 8
- [8] Yuning Cui, Yi Tao, Zhenshan Bing, Wenqi Ren, Xinwei Gao, Xiaochun Cao, Kai Huang, and Alois Knoll. Selective frequency network for image restoration. In *The Eleventh International Conference on Learning Representations*, 2023. 3
- [9] Yann N. Dauphin, Angela Fan, Michael Auli, and David Grangier. Language modeling with gated convolutional networks. In *Proceedings of the 34th International Conference on Machine Learning - Volume 70*, page 933–941. JMLR.org, 2017. 3
- [10] Xiaohan Ding, Xiangyu Zhang, Ningning Ma, Jungong Han, Guiguang Ding, and Jian Sun. Repvgg: Making vgg-style convnets great again. In *Proceedings of the IEEE/CVF Conference on Computer Vision and Pattern Recognition (CVPR)*, pages 13733–13742, 2021. 2
- [11] Alexey Dosovitskiy, Lucas Beyer, Alexander Kolesnikov, Dirk Weissenborn, Xiaohua Zhai, Thomas Unterthiner, Mostafa Dehghani, Matthias Minderer, Georg Heigold, Sylvain Gelly, Jakob Uszkoreit, and Neil Houlsby. An image is worth 16x16 words: Transformers for image recognition at scale, 2021. 1, 2
- [12] Daniel Feijoo, Paula Garrido, Marcos V Conde, Jaesung Rim, Alvaro Garcia, Sunghyun Cho, and Radu Timofte. Efficient real-world deblurring using single images: Aim 2025 challenge report. In *Proceedings of the IEEE/CVF International Conference on Computer Vision*, pages 5713–5721, 2025. 1, 2
- [13] Dan Hendrycks and Kevin Gimpel. Gaussian error linear units (gelus), 2023. 4
- [14] Seo-Won Ji, Jeongmin Lee, Seung-Wook Kim, Jun-Pyo Hong, Seung-Jin Baek, Seung-Won Jung, and Sung-Jea Ko. Xydeblur: Divide and conquer for single image deblurring. In *Proceedings of the IEEE/CVF Conference on Computer Vision and Pattern Recognition (CVPR)*, pages 17421–17430, 2022. 2
- [15] Liming Jiang, Bo Dai, Wayne Wu, and Chen Change Loy. Focal frequency loss for image reconstruction and synthesis. In *Proceedings of the IEEE/CVF International Conference on Computer Vision (ICCV)*, pages 13919–13929, 2021. 2, 5
- [16] Justin Johnson, Alexandre Alahi, and Li Fei-Fei. Perceptual losses for real-time style transfer and super-resolution. In *Computer Vision – ECCV 2016*, pages 694–711, Cham, 2016. Springer International Publishing. 1
- [17] Kwangyoung Kim, Felix Wu, Yifan Peng, Jing Pan, Prashant Sridhar, Kyu J. Han, and Shinji Watanabe. E-branchformer: Branchformer with enhanced merging for speech recognition. In *2022 IEEE Spoken Language Technology Workshop (SLT)*, pages 84–91, 2023. 2, 4
- [18] Lingshun Kong, Jiangxin Dong, Jianjun Ge, Mingqiang Li, and Jinshan Pan. Efficient frequency domain-based transformers for high-quality image deblurring. In *Proceedings of the IEEE/CVF Conference on Computer Vision and Pattern Recognition (CVPR)*, pages 5886–5895, 2023. 2
- [19] Orest Kupyn, Volodymyr Budzan, Mykola Mykhailych, Dmytro Mishkin, and Jiří Matas. Deblurgan: Blind motion deblurring using conditional adversarial networks. In *Proceedings of the IEEE Conference on Computer Vision and Pattern Recognition (CVPR)*, 2018. 1
- [20] Orest Kupyn, Tetiana Martyniuk, Junru Wu, and Zhangyang Wang. Deblurgan-v2: Deblurring (orders-of-magnitude) faster and better. In *Proceedings of the IEEE/CVF International Conference on Computer Vision (ICCV)*, 2019. 8
- [21] Yawei Li et al. Ntire 2022 challenge on efficient super-resolution: Methods and results. In *2022 IEEE/CVF Conference on Computer Vision and Pattern Recognition Workshops (CVPRW)*, pages 1061–1101, 2022. 2
- [22] Yawei Li et al. Ntire 2023 challenge on image denoising: Methods and results. In *Proceedings of the IEEE/CVF Conference on Computer Vision and Pattern Recognition (CVPR) Workshops*, pages 1905–1921, 2023. 2
- [23] Jingyun Liang, Jie Zhang Cao, Guolei Sun, Kai Zhang, Luc Van Gool, and Radu Timofte. Swinir: Image restoration using swin transformer. In *Proceedings of the IEEE/CVF International Conference on Computer Vision (ICCV) Workshops*, pages 1833–1844, 2021. 1
- [24] Ze Liu, Yutong Lin, Yue Cao, Han Hu, Yixuan Wei, Zheng Zhang, Stephen Lin, and Baining Guo. Swin transformer: Hierarchical vision transformer using shifted windows. In *Proceedings of the IEEE/CVF International Conference on Computer Vision (ICCV)*, pages 10012–10022, 2021. 4
- [25] Ilya Loshchilov and Frank Hutter. Sgdr: Stochastic gradient descent with warm restarts, 2017. 6

- [26] Ilya Loshchilov and Frank Hutter. Decoupled weight decay regularization, 2019. 6
- [27] Xintian Mao, Yiming Liu, Fengze Liu, Qingli Li, Wei Shen, and Yan Wang. Intriguing findings of frequency selection for image deblurring. *Proceedings of the AAAI Conference on Artificial Intelligence*, 37(2):1905–1913, 2023. 2
- [28] D. Marr and E. Hildreth. Theory of edge detection. *Proceedings of the Royal Society of London. B. Biological Sciences*, 207(1167):187–217, 1980. 5
- [29] Daniel Morales-Brotons, Thijs Vogels, and Hadrien Hendriks. Exponential moving average of weights in deep learning: Dynamics and benefits. *Transactions on Machine Learning Research*, 2024. 5
- [30] Seungjun Nah, Tae Hyun Kim, and Kyoung Mu Lee. Deep multi-scale convolutional neural network for dynamic scene deblurring. In *Proceedings of the IEEE Conference on Computer Vision and Pattern Recognition (CVPR)*, pages 3883–3891, 2017. 1, 8
- [31] Seungjun Nah et al. Ntire 2021 challenge on image deblurring. In *2021 IEEE/CVF Conference on Computer Vision and Pattern Recognition Workshops (CVPRW)*, pages 149–165, 2021. 2
- [32] Zhiliang Peng, Wei Huang, Shanzhi Gu, Lingxi Xie, Yaowei Wang, Jianbin Jiao, and Qixiang Ye. Conformer: Local features coupling global representations for visual recognition. In *Proceedings of the IEEE/CVF International Conference on Computer Vision (ICCV)*, pages 367–376, 2021. 2
- [33] Jaesung Rim, Haeyun Lee, Jucheol Won, and Sunghyun Cho. Real-world blur dataset for learning and benchmarking deblurring algorithms. In *Computer Vision – ECCV 2020: 16th European Conference, Glasgow, UK, August 23–28, 2020, Proceedings, Part XXV*, page 184–201, Berlin, Heidelberg, 2020. Springer-Verlag. 1, 7
- [34] Jaesung Rim, Geonung Kim, Jungeon Kim, Junyong Lee, Seungyong Lee, and Sunghyun Cho. Realistic blur synthesis for learning image deblurring. In *Computer Vision – ECCV 2022: 17th European Conference, Tel Aviv, Israel, October 23–27, 2022, Proceedings, Part VII*, page 487–503, Berlin, Heidelberg, 2022. Springer-Verlag. 5
- [35] Mark Sandler, Andrew Howard, Menglong Zhu, Andrey Zhmoginov, and Liang-Chieh Chen. Mobilenetv2: Inverted residuals and linear bottlenecks. In *Proceedings of the IEEE Conference on Computer Vision and Pattern Recognition (CVPR)*, 2018. 2
- [36] Wenzhe Shi, Jose Caballero, Ferenc Huszar, Johannes Totz, Andrew P. Aitken, Rob Bishop, Daniel Rueckert, and Zehan Wang. Real-time single image and video super-resolution using an efficient sub-pixel convolutional neural network. In *Proceedings of the IEEE Conference on Computer Vision and Pattern Recognition (CVPR)*, 2016. 3
- [37] Maitreya Suin, Kuldeep Purohit, and A. N. Rajagopalan. Spatially-attentive patch-hierarchical network for adaptive motion deblurring. In *Proceedings of the IEEE/CVF Conference on Computer Vision and Pattern Recognition (CVPR)*, 2020. 2
- [38] Xin Tao, Hongyun Gao, Xiaoyong Shen, Jue Wang, and Ji-aya Jia. Scale-recurrent network for deep image deblurring. In *2018 IEEE/CVF Conference on Computer Vision and Pattern Recognition*, pages 8174–8182, 2018. 8
- [39] Fu-Jen Tsai, Yan-Tsung Peng, Yen-Yu Lin, Chung-Chi Tsai, and Chia-Wen Lin. Stripformer: Strip transformer for fast image deblurring. In *Computer Vision – ECCV 2022*, pages 146–162, Cham, 2022. Springer Nature Switzerland. 2
- [40] Zhengzhong Tu, Hossein Talebi, Han Zhang, Feng Yang, Peyman Milanfar, Alan Bovik, and Yinxiao Li. Maxim: Multi-axis mlp for image processing. In *Proceedings of the IEEE/CVF Conference on Computer Vision and Pattern Recognition (CVPR)*, pages 5769–5780, 2022. 1
- [41] Zhou Wang, A.C. Bovik, H.R. Sheikh, and E.P. Simoncelli. Image quality assessment: from error visibility to structural similarity. *IEEE Transactions on Image Processing*, 13(4): 600–612, 2004. 6
- [42] Zhendong Wang, Xiaodong Cun, Jianmin Bao, Wengang Zhou, Jianzhuang Liu, and Houqiang Li. Uformer: A general u-shaped transformer for image restoration. In *Proceedings of the IEEE/CVF Conference on Computer Vision and Pattern Recognition (CVPR)*, pages 17683–17693, 2022. 2, 7, 8
- [43] Yanchao Yang and Stefano Soatto. Fda: Fourier domain adaptation for semantic segmentation. In *Proceedings of the IEEE/CVF Conference on Computer Vision and Pattern Recognition (CVPR)*, 2020. 2
- [44] Syed Waqas Zamir, Aditya Arora, Salman Khan, Munawar Hayat, Fahad Shahbaz Khan, Ming-Hsuan Yang, and Ling Shao. Multi-stage progressive image restoration. In *Proceedings of the IEEE/CVF Conference on Computer Vision and Pattern Recognition (CVPR)*, pages 14821–14831, 2021. 2, 7, 8
- [45] Syed Waqas Zamir, Aditya Arora, Salman Khan, Munawar Hayat, Fahad Shahbaz Khan, and Ming-Hsuan Yang. Restormer: Efficient transformer for high-resolution image restoration. In *Proceedings of the IEEE/CVF Conference on Computer Vision and Pattern Recognition (CVPR)*, pages 5728–5739, 2022. 1, 2, 4, 8
- [46] Richard Zhang, Phillip Isola, Alexei A. Efros, Eli Shechtman, and Oliver Wang. The unreasonable effectiveness of deep features as a perceptual metric. In *Proceedings of the IEEE Conference on Computer Vision and Pattern Recognition (CVPR)*, 2018. 6
- [47] Zhilu Zhang et al. Ntire 2024 challenge on bracketing image restoration and enhancement: Datasets methods and results. In *Proceedings of the IEEE/CVF Conference on Computer Vision and Pattern Recognition (CVPR) Workshops*, pages 6153–6166, 2024. 2
- [48] Man Zhou, Hu Yu, Jie Huang, Feng Zhao, Jinwei Gu, Chen Change Loy, Deyu Meng, and Chongyi Li. Deep fourier up-sampling. In *Advances in Neural Information Processing Systems*, pages 22995–23008. Curran Associates, Inc., 2022. 3